REPORT

Earth Sciences and Environmental Technologies Division

Study	MPN12	**Division chrono**	R164/n°21/015
Partners		**Contract**	1997C0022

Title	**Assuring integrity of CO2 storage sites through ground surface monitoring (SENSE) – WP2.1: Presentation of conceptual models (Delivrable D2.1)**		
Author(s) and membership	BOUQUET Sarah, ESTUBLIER Audrey, FOURNO André, FREY Jérémy, MALINOUSKAYA Iryna		
Diffusion	Public	**Publication date**	1/10/2021
Division visa *Scientific authentication*	HERZHAFT Benjamin	**Project visa** *Specification compliance*	ESTUBLIER Audrey

Keywords	CO2 storage integrity - Conceptual models

Summary

The project, SENSE, is funded through the ACT program (Accelerating CCS Technologies, Horizon2020 Project No 294766). Its objective is to demonstrate how surface displacements can be used in a monitoring program aimed at verifying the long-term integrity of a CO_2 geological storage site. IFPEN participates as WP2 (work package) leader to coordinate the flow/geomechanics coupling simulation activities in order to understand the surface displacement mechanism in response to pressure changes due to CO_2 injection. In WP2, IFPEN works both on the conceptual models and simulation activities with synthetic cases and real cases.

This report describes all conceptual models and associated properties used in the work package 2.2. Conceptual models without fault are firstly presented. Three sedimentary scenarios inspired from real reservoirs are considered. For each reservoir, an anticlinal is modeled while their properties are related to the Brindisi, In Salah or Snøhvit reservoir. The scenarios with faults are secondly presented and derived from the sedimentary reservoirs. Finally, six corner point grids are obtained. Three grids are used for the sedimentary scenarios and the three others are used for the faulted cases. Considering the faulted cases, the grids present different properties considering different realistic geological cases. The use of the same grid to mimic different geological cases will be useful for a comparison objective in the work package 2.2.

Earth Sciences and Environmental Technologies Division

Diffusion list (pdf)	E-mail address
DELPRAT-JANNAUD Florence	
SOUQUE Christine	
ESNAULT Vivien	
GERVAIS-COUPLET Véronique	
HERZHAFT Benjamin	
CACAS-STENTZ Marie-Christine	
REINERT BRUCH André	
BOHLOLI Bahman (NGI)	Bahman.Bohloli@ngi.no
BOUXIN Alix (ADEME)	alix.bouxin@ademe.fr

For agreement,

Benjamin HERZHAFT :
Accord du Directeur de la Direction Sciences de la Terre et Technologies de l'Environnement

Earth Sciences and Environmental Technologies Division

Table of contents

Earth Sciences and Environmental Technologies Division

Project information

Project title: Assuring integrity of CO_2 storage sites through ground surface monitoring (SENSE)
Project period: 1 September 2019-30 August 2022
Project Coordinator: Norwegian Geotechnical Institute
Web-site: https://sense-act.eu/

Deliverable No.:	D2.1	***Responsible for deliverable:***	NGI
Quality control by:	IFPEN, Frederic Roggero	***Contributing partner(s):***	IFPEN
Deliverable prepared by:	BOUQUET Sarah, ESTUBLIER Audrey, FOURNO André, FREY Jérémy, MALINOUSKAYA Iryna	***Dissemination level:***	Open Access
Project No.:	299664	***Date: 2021-10-01***	Rev. No.: 0

This project, SENSE, is funded through the ACT programme (Accelerating CCS Technologies, Horizon2020 Project No 294766). Financial contributions made from The Research Council of Norway, (RCN), Norway, Gassnova SF (GN), Norway, Bundesministerium für Wirtschaft und Energie (BMWi), Germany, French Environment & Energy Management Agency (ADEME), France, US-Department of Energy (US-DOE), USA, Department for Business, Energy & Industrial Strategy (BEIS) together with extra funding from NERC and EPSRC research councils, United Kingdom, Agencia Estatal de Investigación (AEI), Spain, Equinor and Quad Geometrics are gratefully acknowledged.

1 Introduction

This report describes all conceptual models and associated properties used in Bouquet et al. 2021a and the work package 2.2 (Bouquet et al. 2021b). Conceptual models without fault are firstly presented. Three sedimentary scenarios inspired from real reservoirs are considered. For each reservoir, an anticlinal is modeled while their properties are related to the Brindisi, In Salah or Snøhvit reservoir. The scenarios with faults are secondly presented and derived from the sedimentary reservoirs. To build the synthetic cases including faults and throws, the geometry of the anticline model is preserved while the mesh is adapted to take the new geological structures (faults and throws) into account. Three faults are explicitly modeled; two deterministic faults associated to a throw and a sub-seismic fault without throw. In addition to the three sedimentary scenarios, different flow comportments related to the faults, “open faults” or “sealing faults”, are considered. “Open faults” means that fluids may flow through the faults versus a “sealing faults” for which no-flow occurs through faults but may flow along the fault planes. Six scenarios will be investigated considering faulted cases while only three considering sedimentary cases without fault.

2 Structural conceptual models

Two structural models are considered in this study as potential structures for CO_2 storage. The first one is an anticline structure without fault shown in Figure 1 and Figure 2 (left), and the second one is an anticline structure with faults shown in Figure 1 and Figure 2 (right). The faults are either sealing or draining. The sealing faults represent a barrier for the flow, while the draining faults let flow go through the core zone. Two main faults are defined with a throw in between 6 and 9 kilometers from the well. A third fault is defined as sub-seismic fault without throw and close by about 1.5 kilometers to the well. This sub-seismic fault is representative of such problematic geological objects, often undetectable by geophysical tools, that may behave in unpredictable ways.

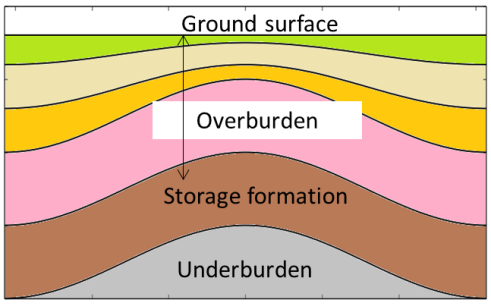

Figure 1 : Schematic representation of the anticline model

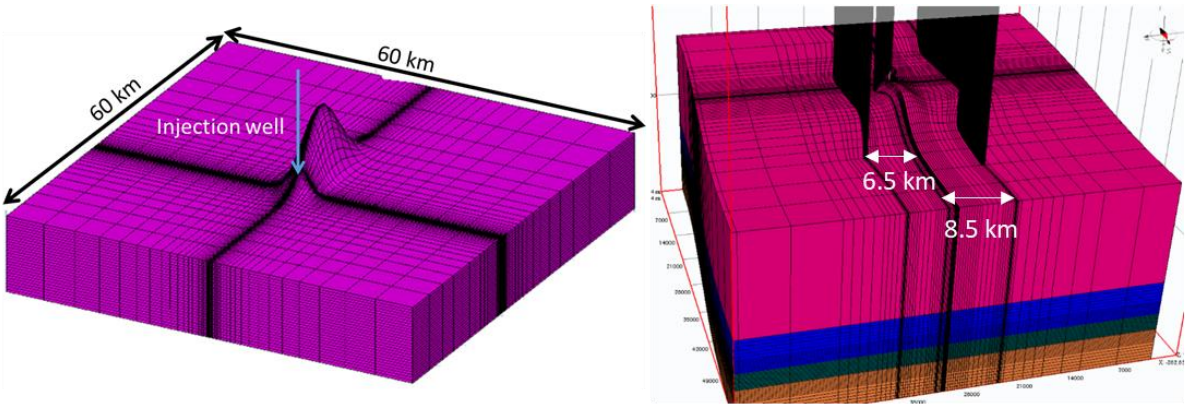

Figure 2 : Anticline conceptual models. Left, anticline trap without fault; right, anticline trap with two major faults and a sub-seismic fault.

Model dimensions are about 60×60 km^2. The anticline structure is in the center of the grid, the well is 6 km from the top of the fold (Figure 2). The anticline structure extends over 10 km in Y-direction and over 3 km in X-direction. The fold intensity is defined by its thickness, i.e. the highest difference in depth for a same layer, of 50 m.
A tartan grid was defined with refinement close to the well. The lateral mesh size is 51 x 51 cells with 50 x 50 m for the smallest cell size. Only a bottom part of the overburden (Table 2) is taken into account to model the flow. A weak flow may occur in this active part. For geomechanical simulations, the models include all layers from the bottom of the storage formation (underburden) up to the surface (e.g. Figure 1). The vertical mesh size depends on the storage formation thickness and consequently on the properties of subsurface scenarios (see paragraph 3) since the vertical discretization is kept constant in the storage formation: 2 m. Thus, the number of layers in the storage

formation varies between 25 and 100 layers. Five layers represent the underburden of 10 m height, 15 layers represent the caprock and the overburden up to the surface.

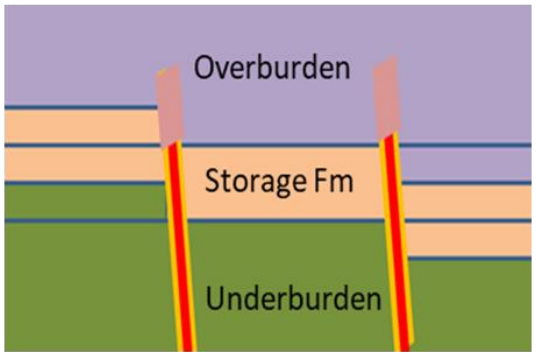

Faults (core and damage zones) with throw

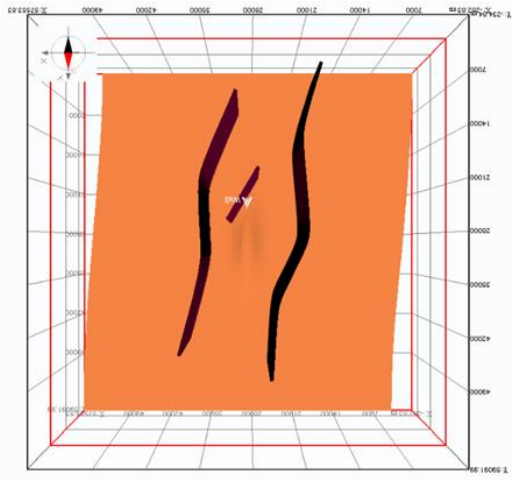

Figure 3 : Conceptual model with faults. Left, schematic representation of the main faults with throw and with explicit modelling of core and damage zones. Right, top view of fault models with two main faults and the smallest and closest sub-seismic fault.

3 Sedimentary deposits contexts for conceptual models

Several scenarios are considered to represent different types of sedimentary formations and therefore corresponding to different subsurface properties. These scenarios are defined to generate realistic intervals of uncertainty of the properties. Three scenarios are defined.

- **Carbonate Case**, inspired from Brindisi (Baroni et al., 2015) and Michigan Basin (MRCSP Michigan Basin, Michael et al., 2010) storage sites.
- **Sandstone I case**, inspired from In Salah (Baroni et al., 2011; Deflandre et al., 2013; Tremosa et al., 2014) and Gorgon (Michael et al., 2010; Flett et al., 2008; Schembre-McCabe et al. 2008) projects.
- **Sandstone II case**, inspired from Snøhvit (Estublier et al. 2009; Niemi et al. 2017), Decatur (Mt Simon, Zhou et al. 2010; Ruqvist et al. 2019) and Otway (Cook 2014) storage sites.

Pressure and temperature conditions, salinity, storage depth and thickness, petrophysical properties, mechanical properties of the storage formation and of the overlying and underlying formations are defined from the collected data.
Nine of these properties are considered as critical and uncertain including the porosity, permeability, Young modulus and Poisson ratio properties of the storage formation and overburden (caprock), as well as the capillary CO_2 entry pressure of the caprock. These uncertain parameters are defined through uncertainty intervals determined from the collected information. The *a priori* distribution of the parameter values corresponds to a uniform law on the defined uncertainty interval. Table 1 gives the range of values for those uncertain parameters for all cases. For example, the most significant difference between sandstones cases is their injectivity properties. Other properties are set at specific values, defined in Table 2.

Variables – Uncertain parameters	Carbonates Min -Max	Sandstone I Min-Max	Sandstone II Min-Max
Storage Fm Porosity [-]	0.15 – 0.25	0.1 – 0.3	0.1 – 0.2
Storage Fm Permeability [mD]	15 – 150	5 – 50	100 - 1000
Storage Fm Young Modulus [GPa]	25 – 45	2 – 15	5 – 20
Storage Fm Poisson coefficient [-]	0.15 – 0.25	0.2 – 0.3	0.15 – 0.25
Overburden Porosity [-]	0.05 – 0.4	0.05 – 0.15	0.05 – 0.15
Overburden Permeability [mD]	2e-3 – 6e-2	1e-3 – 1e-1	1e-4 – 1e-2
Overburden Entry Capillary Pressure [bar]	5 – 60	10 – 50	5 - 50
Overburden Young Modulus [GPa]	6 – 55	1 – 20	30 – 40
Overburden Poisson coefficient [-]	0.15 – 0.35	0.2 – 0.35	0.2 – 0.3

Table 1 : Uncertain parameters and related ranges of values for the three scenarios

Fixed parameters	Carbonate	Sandstone I	Sandstone II
Depth [m]	1600	1800	2000
P, T [bar, °C]	160; 40	180; 90	200; 80
Storage Fm Thickness [m]	50	200	100
(active) Overburden Thickness [m]	100	800	80
Salinity [mg/L]	35 000	150 000	120 000
Anisotropy (Kv/Kh)	0.1	0.1	0.8

Table 2 : Fixed values for some storage properties for the three scenarios

Cohesion and friction values are calculated as a function of sedimentary formations (carbonate and sandstone for reservoir, clay and marl for caprock) and porosity values as described in paragraph 2 and with the following specificities.

- For carbonate, empirical coefficients are directly identified from experimental data (Bemer and al. 2004).
- For sandstone, empirical coefficients have been adapted from Bemer and al. 2004 available data.
- For clay, empirical coefficients are deduced from available literature data (Hu and al., 2014), (Menaceur and al. 2015), (Bossart, 2008).
- For marl, we consider a composition of 60% clay and 40% carbonate, empirical coefficients are then calculated as a composition weighted average ($\alpha^{marl} = 0.6\,\alpha^{clay} + 0.4\,\alpha^{carbonate}$) .

Identified empirical coefficients are summarized in Table 3, Table 4 and Table 5 :

	α_c	β_c	α_f	β_f
Carbonate	40.3	-0.054	-0.893	49
Sandstone	37.9	-0.09	0	20.78
Clay	9.1	-0.062	0	21
Marl	21.6	-0.059	-0.357	32.2

Table 3 : Identified empirical coefficients for Carbonate, Sandstone, Clay and Marl (see paragraph 2)

	Porosity - Marls [%]	Cohesion [MPa] - Marls	Friction angle [°] - Marls
Min.	5.09	2.05	17.91
Median	22.40	5.77	24.19
Max.	39.99	15.99	30.38

Table 4 : Marls – Porosity, cohesion and Friction angle

	Porosity [%] - Clay	Cohesion [MPa] - Clay	Friction angle [°] - Clay
Min.	5.02	3.59	21
Median	9.97	4.90	21
Max.	14.99	6.66	21

Table 5 : Clay – Porosity, cohesion and Friction angle

4 Scenarios with faults

4.1 Geological structures

To build the synthetic cases including faults and throws, the geometry of the anticline model is preserved while the mesh is adapted to take the new geological structures into account. A conceptual model including faults is defined (Figure 4) to build new faulted scenarios. Three faults are explicitly modeled; two deterministic faults (DF) associated to a throw and a sub-seismic fault (SSF) without throw. For each scenario previously defined (Carbonate, Sandstone I and Sandstone II), we add two characteristics related to the faults with an “open faults” and “sealing faults” cases. “Open faults” means that fluids may flow through the faults versus a “sealing faults” for which no-flow occurs through the faults. Each fault is explicitly modelled with a fracture corridor (damaged zone) and a fault core. These corridors of fractures have a major impact on the CO_2 volume storage and on flow. Moreover, for sealing faults, the injected CO_2 may flow along the fault planes but not through the fault. These fault impacts on the flow are commonly observed (Skerlec 1999). To summarize, the following cases are considered:

- Homogeneous reservoirs without faults and throws. This case will be used as a comparison case.
- Open faults behavior, the CO_2 may flow through the faults. The throws are associated to the deterministic faults and explicitly modeled.
- Sealing faults behavior, the CO_2 does not flow through the faults but may flow along the fault planes. The throws are associated to the deterministic faults and explicitly modeled.

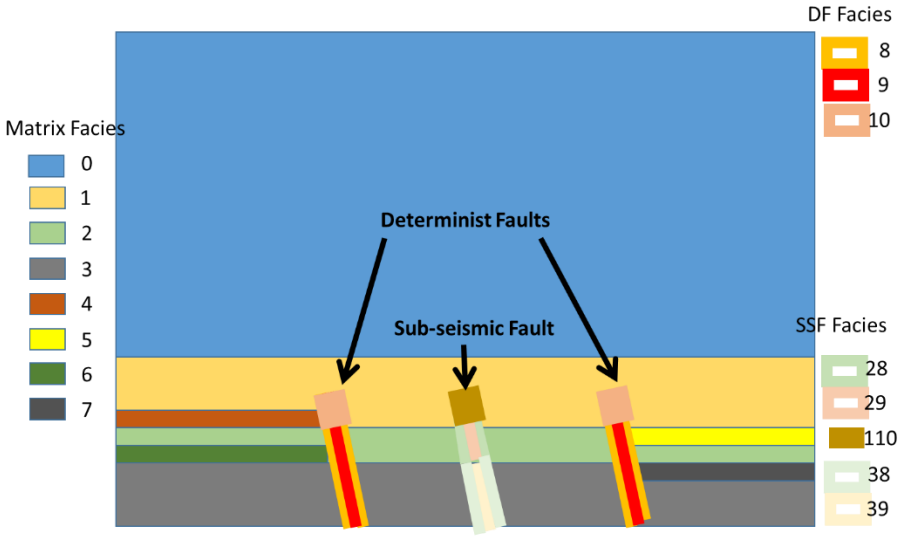

Figure 4 : Conceptual model of faulted scenarios. Facies are defined to quickly build different realistic configurations thanks to an adapted choice of properties values. Facies 4 to 7 are used to model the throws or not. Facies 9, 29 and 39 are used to define a fault core and are useful to model open faults or sealing faults. Facies 8, 28 and 38 are used to model a fracture corridor associated to the faults.

To easily model the fault impacts on flow, the faults are explicitly meshed. More precisely a fault is modeled using 4 cell thicknesses (Figure 5).

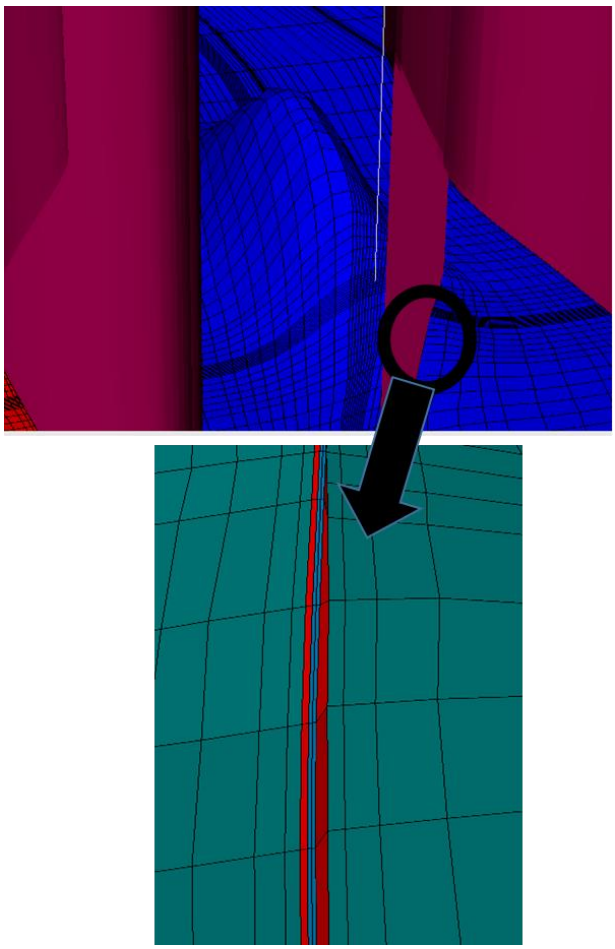

Figure 5 : Anticlinal and faults with a zoom to illustrate the fault mesh

Based on this fault mesh, open or sealing faults are modeled using respectively a huge or a weak fault core permeability value as illustrated Figure 6. Indeed, a weak permeability value of the core fault zone implies a weak transmissibility value and therefore may create a flow barrier.

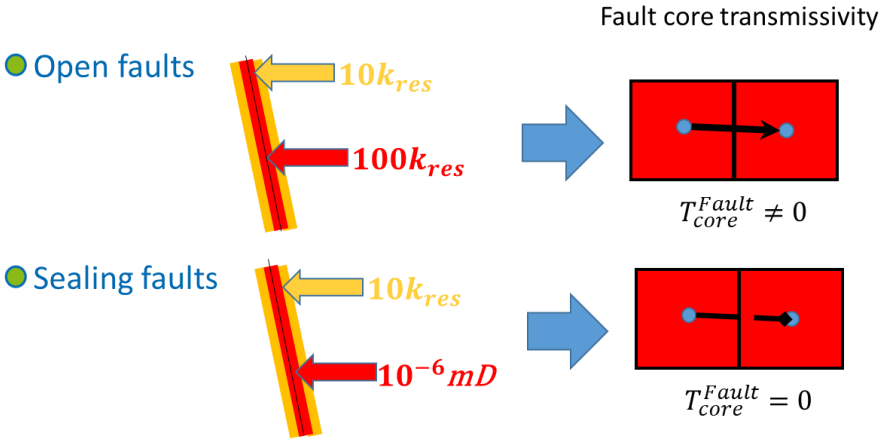

Figure 6 : Permeability value associated to an open or a sealing fault

In addition, facies heterogeneities may be added to the fault models. Two facies are defined in both the storage formation and the overburden. A truncated-gaussian approach (Doligez et al., 2011) is used to model their distributions. Two gaussian functions are used and associated to exponential variograms whose ranges are about 3 km and 7 km respectively for the reservoir and the overburden. The facies contact rules are defined by square pictures (Figure 7b, c, d). These squares define a contact rule graph whose x axe is associated to the first gaussian function while y axe is associated to the second gaussian function. Thresholds used to define the proportions of facies are given by pie charts. Our model is simplest than illustrated by the Figure 7. The reservoir facies distribution is simply associated to the first gaussian function while the overburden facies distribution is associated to the second one.

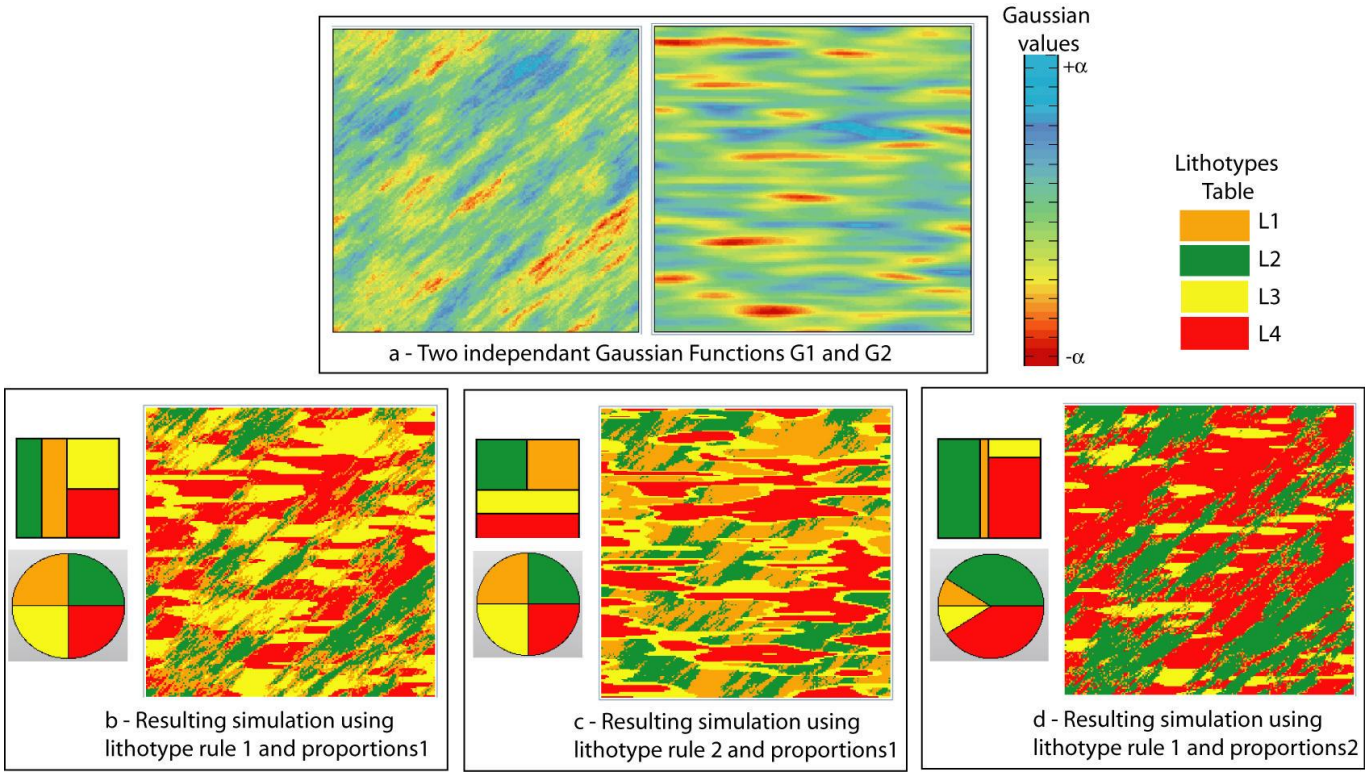

Figure 7 : Summary of the pluri-gaussian method and parameters: two Gaussian functions (a), different lithotype rules (b and c); different lithotype proportions (b and d) and resulting lithotype simulations (from Doligez et al., 2011)

The result of this modeling is illustrated Figure 8. The coarse distribution far from the well is due to a meshing effect.

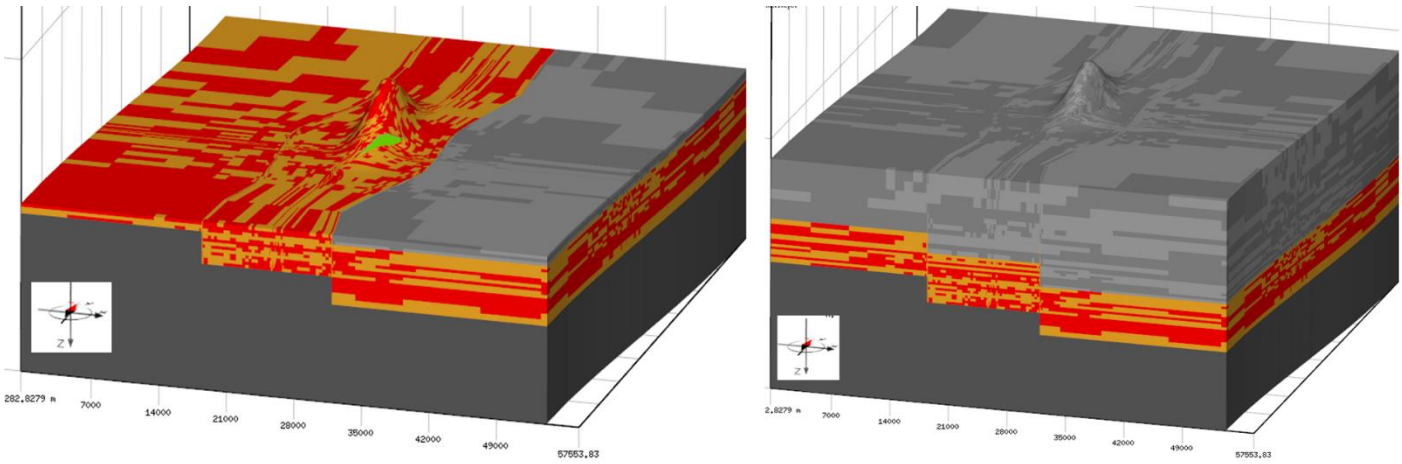

Figure 8 : result of a heterogenous modeling for reservoir and overburden

4.2 Property values

To define the properties of both the storage formation facies and the overburden facies, we use the median values from the uncertain interval defined previously. Main property values are given in the Table 6, for each no-faulted scenario. The “main” property values are used for both homogeneous and heterogeneous cases (first facies). The “second” property values are only used for heterogenous cases for the second facies. The flow properties of the heterogeneous reservoir are improved with a more porous and permeable second facies while the overburden is more impermeable by using a less permeable and porous second facies. The chosen fault properties are related to the reservoir properties as illustrated in Figure 6 and indicated in Table 7. For the fault core and corridor media, the relative permeability curves form a cross curve while a null value is taken as capillarity pressure values. Mechanical fault properties are calculated considering the fault porosity values.

Variables	Carbonates Main / Second facies	Sandstone I Main/Second facies	Sandstone II Main/Second facies
Storage Fm Porosity [-]	0.2 / 0.3	0.2 / 0.3	0.15 / 0.2
Storage Fm Permeability [mD]	47.4 / 70	15.8/30.	316 / 500
Storage Fm Young Modulus [GPa]	35 /27	8.5 / 7	12.5 / 11
Storage Fm Poisson coefficient [-]	0.2 / 0.2	0.25 / 0.25	0.2 / 0.2
Overburden Porosity [-]	0.15/0.1	0.1/0.05	0.1 / 0.05
Overburden Permeability [mD]	1.1e-2 / 5e-3	1e-2 / 5e-3	1e-3 / 5e-4
Overburden Entry Capillary Pressure [bar]	41	36	35
Overburden Young Modulus [GPa]	30.5 /34	10.5 / 11.5	35 / 39
Overburden Poisson coefficient [-]	0.25 / 0.25	0.275 / 0.275	0.25 / 0.25

Table 6 : Parameter values for each facies for the three scenarios

Variables	Carbonates Corridor / Core	Sandstone I Corridor / Core	Sandstone II Corridor / Core
Fault Porosity [-]	0.35 / 0.35		
Fault Permeability [mD]	474 / 4740	158 / 1580	3160 / 31600
Fault Young Modulus [GPa]	17.5 / 17.5	4.25 / 4.25	6.25 / 6.25
Fault Poisson coefficient [-]	0.2 / 0.2	0.25 / 0.25	0.2 / 0.2

Table 7 : Fault parameter values (corridor / core) for the three scenarios

Finally, for each scenario (Carbonate, Sandstone I and Sandstone II), it is now possible to study different realistic geological cases:

- sealing fault for the homogeneous case,
- sealing fault for the heterogeneous case,
- open fault for the homogeneous case,
- open fault for the heterogeneous case,
- homogeneous case without fault and without throw.

5 Conclusions

Finally, six corner point grids are obtained. Three grids are used for the sedimentary scenarios and the three others are used for the faulted cases. Nevertheless, caprock, reservoir and underburden grid properties are always related to the associated real reservoir. In addition, considering the faulted cases, the grids may also present different grid properties considering different realistic geological cases:

- sealing fault for the homogeneous case,
- sealing fault for the heterogeneous case,
- open fault for the homogeneous case,
- open fault for the heterogeneous case,
- homogeneous case without fault and without throw.

The use of the same grid to mimic different geological cases will be useful for a comparison objective in the work package 2.2 (Bouquet et al. 2021b). Consequently, considering each faulted grid, five grid properties may be used depending on geological cases.

6 Bibliography

Baroni, A., Estublier, E., Deflandre, J.-P., Daniel, J.-M. (2011). Modelling surface displacements associated with CO_2 reinjection at Krechba. 45th US Rock Mechanics / Geomechanics Symposium.

Baroni, A., Estublier, A., Vincké, O., Delprat-Jannaud, F., Nauroy, J-F., (2015). Dynamic Fluid Flow and Geomechanical Coupling to Assess the CO_2 Storage Integrity in Faulted Structures. Oil & Gas Science and Technology - 70 (4), pp.729-751.

Bemer, E., Vincké, O., and Longuemare, P. (2004): Geomechanical Log Deduced from Porosity and Mineralogical ContentOil & Gas Science and Technology - Rev. IFP, 59 4, 405-426.

Bouquet, S., Frey, J., Malinouskaya, I., Soulat, A., Estublier, A., Fourno, A., (2021a). Analysis of Surface Movement through Conceptual and Coupled Flow-Geomechanics Models an Example of Surface Monitoring Assessment for CCS Project. SINTEF Proceedings;7, Chapter.

Bouquet S., Estublier, A., Fourno A., Frey J., Malinouskaya, I., (2021b). Assuring integrity of CO2 storage sites through ground surface monitoring (SENSE) – - WP2.2: Understanding the mechanism of surface movement (Deliverable D2.2).

Bossart, P., Jaeggi, D., Nussbaum, C. (2008) Experiments on thermo-hydro-mechanical behaviour of Opalinus Clay at Mont Terri rock laboratory, Switzerland - Journal of Rock Mechanics and Geotechnical Engineering, Volume 10, Issue 6, December 2018, Pages 1190

Cook, P.J., (2014). Geologically Storing Carbon: Learning from the Otway Project Experience. CSIRO Publishing, Melbourne, ISBN: 978-1-118-98618-9.

Doligez, B., Hamon, Y., Barbier, M., Nader, F., Lerat, O., Beucher, H., 2011. Advanced workflows for joint modeling of sedimentary facies and diagenetic overprint. In: Impact on reservoir quality. SPE Paper #SPE-146621, SPE Annual Technical Conference and Exhibition, Denver, Colorado, USA.

Deflandre, J.-P., Estublier, A., Baroni, A., Fornel, A., Clochard, V., Delépine, N. (2013). Assessing field pressure and plume migration in CO_2 storages: Application of case-specific workflows at in Salah and Sleipner. Energy Procedia, 37, pp. 3554-3564. doi: 10.1016/j.egypro.2013.06.248

EDF. Code_aster, Analyse des Structures et Thermo-mécanique pour des Études et des Recherches. www.code-aster.org [consulté le 05/10/2020]

Estublier, A., Lackner, A.F.(2009). Long-term simulation of the Snøhvit CO_2 storage, Energy Procedia, Volume 1, Issue 1, Pages 3221-3228, ISSN 1876-6102, https://doi.org/10.1016/j.egypro.2009.02.106.

Flett, M. et al. (2008). Gorgon Project: Subsurface evaluation of carbon dioxide disposal under Barrow Island. SPE Asia Pacific Oil and Gas Conference, Perth, Australia, October 20-22 . SPE 116372.

Hu DW, Zhang F, Shao JF. (2014): Experimental study of poromechanical behavior of saturated claystone under triaxial compression Acta Geotechnica; 9:207-214.

IFP Energies nouvelles (2018). PumaFlow 10.0 reference manual. France.

Menaceur H, Delage P, Tang A-M, Conil N (2015) The thermo-mechanical behaviour of the Callovo–Oxfordian claystone. Int J Rock Mech Min Sci 78:290–303.

Michael, K., Golab, A., Shulakova, V., Ennis-King, J., Allinson, G., Sharma, S., Aiken, T (2010). Geological storage of CO_2 in saline aquifers-A review of the experience from existing storage operations, International Journal of Greenhouse Gas Control, 4 (4), pp. 659-667. doi: 10.1016/j.ijggc.2009.12.011

Niemi, A., Bear, J., Bensabat, J. (2017). Geological Storage of CO_2 in Deep Saline Formations, Volume 29 de Theory and Applications of Transport in Porous Media, Springer.

Rutqvist, J., Rinaldi, A. P., Vilarrasa, V., Cappa, F. (2019). Chapter 10 - Numerical Geomechanics Studies of Geological Carbon Storage (GCS), Editor(s): Pania Newell, Anastasia G. Ilgen, Science of Carbon Storage in Deep Saline Formations, Elsevier, Pages 237-252, ISBN 9780128127520, https://doi.org/10.1016/B978-0-12-812752-0.00010-1.

Schembre-McCabe, J.M., Kamath, J., Gurton, R. (2008). Mechanistic Studies of CO_2 Sequestration. International Petroleum Technology Conference. Dubai, UAE, December 4-6. IPTC 11391.

Schweizer, D., Blum, P., Butscher, C. (2017). Data assimilation and uncertainty assessment in 3D geological modeling. Solid Earth Discussions, 1-23.

Skerlec, G.M., (1999). Treatise of Petroleum Geology / Handbook of Petroleum Geology: Exploring for Oil and Gas Traps. Chapter 10: Evaluating Top and Fault Seal, AAPG Special Volumes. https://wiki.aapg.org/Fault_seal_behavior

Tremosa, J., Castillo, C., Vong, C.Q., Kervévan, C., Lassin, A., Audigane, P. (2014). Long-term assessment of geochemical reactivity of CO_2 storage in highly saline aquifers: Application to Ketzin, In Salah and Snohvit storage sites. International Journal of Greenhouse Gas Control,Elsevier, 2014, 20, pp.2-26..

Zhou, Q., Birkholzer, J.T., Mehnert, E., Lin, Y.-F. and Zhang, K. (2010), Modeling Basin- and Plume-Scale Processes of CO_2 Storage for Full-Scale Deployment. Groundwater, 48: 494-514. doi:10.1111/j.1745-6584.2009.00657.x

Annex A - Tables

1. Figures table

2. Tables table